PHENOMENOLOGICAL COMPARISON OF MAGNETIC AND ELECTROSTATIC FLUCTUATIONS IN THE MACROTOR TOKAMAK

S.J. ZWEBEN*, R.J. TAYLOR
Tokamak Fusion Laboratory,
University of California, Los Angeles,
Los Angeles, California,
United States of America

ABSTRACT. Probe measurements of magnetic and electrostatic fluctuations in Macrotor are compared. Attention is concentrated on small-scale fluctuations which lie in the frequency range above the usual low-frequency Mirnov oscillations. In this range, 20 kHz $< f <$ 125 kHz, the spectra of $\tilde{B}$ and $\tilde{\phi}$ are similar; the radial profile of $\tilde{n}/n$ is, however, peaked toward the outside while that of $\tilde{B}_r$ is peaked toward the centre, and no local cross-correlation between $\tilde{B}$ and $\tilde{\phi}$ has been detected. The radial correlation length of $\tilde{\phi}$ is smaller than that for $\tilde{B}_r$ (both being much smaller than the minor radius), but the poloidal correlation lengths of $\tilde{B}_p$ and $\tilde{\phi}$ are similar. Both $\tilde{B}$ and $\tilde{\phi}$ fluctuations rotate in the electron diamagnetic drift direction. The spectra are roughly invariant to an increase in density; however, the magnitude of $\tilde{n}/n$ decreases with density while that of $\tilde{B}_r$ remains unchanged. No connection between these fluctuations and anomalous transport has been established.

1. INTRODUCTION

In a previous publication [1], we reported the observation of small-scale broadband magnetic fluctuations in the Macrotor tokamak. In the present paper, we describe in more detail probe measurements of electrostatic fluctuations in Macrotor, and present evidence indicating that there is apparently no clear-cut connection between these electrostatic and magnetic fluctuations in the range 20 kHz$<f<$125 kHz.

Interest in tokamak fluctuations centres on proposed explanations for the anomalously large electron heat conduction observed in the experiments. Scattering [2–4] and probe [1, 5, 6] measurements in tokamaks have shown a 'turbulent' spectrum of the density fluctuations; typically, $\tilde{n}/n \cong 10^{-3}$ to 10^{-1}; however, the interpretation of these results in terms of transport is difficult and uncertain [7]. Probe measurements in tokamaks [1, 8, 9] have shown a broadband spectrum of magnetic fluctuations (at frequencies above the usual Mirnov oscillations) with $\tilde{B}_r/B_T \cong 10^{-4}$, and although there are several theories which indicate that such a level of $\tilde{B}$ could exist in tokamaks and could account for the anomalous transport [10–21], no detailed connection between theory and experimental measurements of $\tilde{B}$ fluctuations has yet been made.

Our approach in the present paper has been purely phenomenological, i.e. we have not yet attempted a detailed comparison between these measurements and theory. This is in part due to the intrinsic complexity of the observed phenomena which, for instance, do not encourage interpretations based on a linear MHD model (in which $\tilde{B}$ and $\tilde{\phi}$ would be simply correlated). Although more subtle theoretical models are being developed, we believe that the incomplete state of both theory and experiment are such that a convincing fit between the two cannot yet be made (this should not be too surprising given the unresolved state of other tokamak instability phenomena).

2. EXPERIMENTAL DETAILS

Macrotor [22] is a large (R = 90 cm, a = 45 cm), low-field ($B_T \cong 2$–3 kG), and, therefore, low-power-density tokamak ($T_{e0} \cong 100$ eV, $n \cong 10^{12}$-10^{13} cm^{-3}), into which probes can be inserted to measure the local magnetic and electrostatic fluctuations directly (see Table I). In the present experiments, we have used magnetic and capacitive probes inside ≅2-cm-diameter glass tubes inserted, typically, 5–15 cm past the limiter near the equatorial plane.

The capacitive probes measure electrostatic potential fluctuations $\tilde{\phi}_c$ and are mounted just outside the electrostatic shields of magnetic probes (Fig.1) in

* Present address: 116–81, Caltech, Pasadena, California 91125, USA.

TABLE I. MACROTOR PARAMETERS

R	= 90 cm
a	= 45 cm (chamber)
I	= 60 kA
pulse length	>50 ms
B_T	= 2–3 kG
q(a)	= 3–4
V_{loop}	= 1–2
Z_{eff}	≅ 1
T_{e0}	≅ 100 eV
T_{i0}	≅ 50 eV
n_e	≅ 10^{12}–10^{13} cm^{-3}
τ_E	≅ 0.5–5 ms (accords with na^2 empirical scaling)
β_{peak}	= 0.1–1%
ρ_i	= 0.3 cm
λ_D	= 3×10^{-3} cm
λ_B	= c/ω_p ≅ 0.3 cm

order to compare $\tilde{B}$ and $\tilde{\phi}_c$ at a 'point'. We have also measured floating-potential $\tilde{\phi}_f$ and density fluctuations $\tilde{n}$ with Langmuir probes located near the tubes containing the $\dot{B}$ coils, and have investigated the spatial structure of $\tilde{\phi}_f$ using a pair of movable Langmuir probes. Note that the probes are inserted well into the plasma, but not quite to the highest-power-density region near the minor axis.

The capacitive probes [23] respond to the floating-potential fluctuations in the plasma just outside the glass tube surrounding the probe; presumably, the glass itself acts as a passive insulation and does not distort the capacitive coupling between the plasma and the probe electrode. These probes have been used to measure only the spectrum and not the absolute value of the electrostatic-potential fluctuations (the value of the capacitive probes is mainly that they can be placed very close to the magnetic pick-up loops in order to compare $\tilde{\phi}$ with $\tilde{B}$ locally). The Langmuir-probe floating-potential fluctuation spectrum is identical with that recorded by the capacitive probes, and the absolute value of the floating-potential fluctuations $\tilde{\phi}_{f,rms}$ can be measured in this way.

The Langmuir probes have also been used in their electron or ion saturation regimes to study density fluctuations. We have not used the Langmuir probes to measure temperature or absolute density since this would require consideration of the details of probe theory in a magnetic field. In these saturation current regimes, only the relative density fluctuation $\tilde{n}/n$ can be evaluated easily (see Section 4.1).

The $\dot{B}$ probes are constructed in the usual way, including a thin electrostatic shield (Fig.1). The absence of capacitive coupling to the magnetic probes has been checked *in situ* by rotating one of two nearby coils 180° and noting the 180° phase shift. The absence of interference between the $\tilde{B}$ and $\tilde{\phi}_c$ signals has also been checked, along with the linearity of the probes and amplifiers to ≳150 kHz. The signals are stored on a multichannel magnetic drum which records the whole shot (≲100 ms) with a ≳150-kHz bandwidth. The drum signals are low-pass-filtered (f < 125 kHz) to prevent aliasing and are digitized with a 4-μs ADC and Fourier-analysed by computer in the usual way.

The absence of probe-induced perturbations has been checked as previously [1]; for example, the introduction of the probes is seen not to affect any macroscopic properties of the discharge (the probes become 'conditioned' or cleaned up after a few tokamak discharges, and the runaway level was generally low

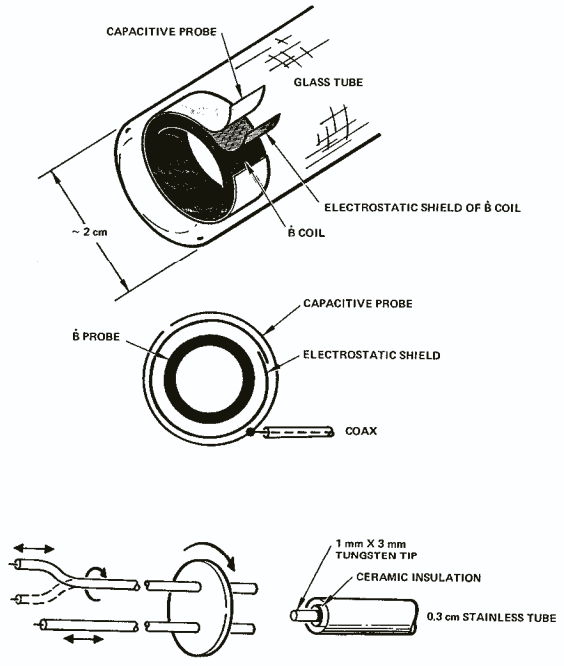

FIG.1. Probe construction: The $\tilde{B}$ coil is 1 cm × 0.3 cm and 20 turns, surrounded by a thin aluminium-foil electrostatic shield which itself is nearly covered by a thin copper (broken) ring electrode of the capacitive probe. The $\tilde{B}$ signal is differentially amplified × 100, and the capacitive probe signal is monitored with 1 MΩ to ground by a voltage follower.

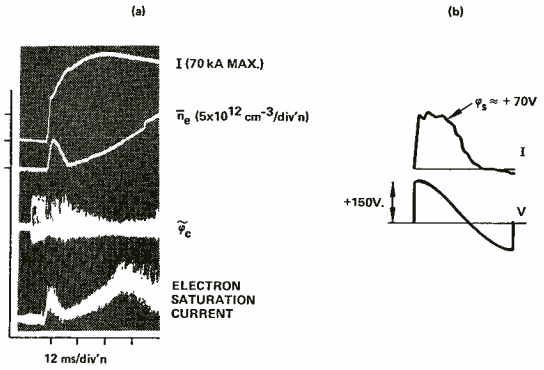

FIG.2. Electrostatic fluctuations: a) Typical signals of capacitive probe and of electron saturation current of Langmuir probe (V = +200 V) during a discharge in which the density is increased by gas puffing. Note that the probes respond to the breakdown oscillator at t < 0. b) Typical Langmuir probe characteristic is shown, here for a probe 10 cm inside the RF antenna boundary. The spectrum and relative value of $\tilde{n}_e$ and $\tilde{n}_i$ fluctuations are identical (indicating that secondary electron emission is not significant for $\tilde{n}_i$).

enough to avoid probe damage). In addition, the similarity between the $\tilde{\phi}$ spectrum measured with capacitive and Langmuir probes, the simple character of the (V, I) Langmuir characteristic (see Section 4.1), and the lack of effect of one Langmuir probe on another nearby Langmuir probe – all this points to the non-perturbing nature of the electrostatic measurements. It should, however, be noted that probe measurements can generally not be accorded the same degree of certainty as, for example, the intrinsically non-perturbative scattering measurements.

We shall first describe some characteristics of electrostatic fluctuations in Macrotor and then turn to a comparison of these with magnetic fluctuations.

3. ELECTROSTATIC FLUCTUATIONS

Figure 2a shows traces of the electron saturation current measured with a Langmuir probe and $\tilde{\phi}_c$ measured by the capacitive probe, along with plasma current and line-averaged density through the centre of the plasma. Both probes are located, in this case, about 5 cm inside the boundary defined by the outer limiter, which for these experiments was a vertical RF antenna extending 15 cm inside the chamber wall at a point 60° toroidally from the probes (the antenna itself extends only ~10 cm in the toroidal direction, thus producing a very diffusive limiter shadow at the probes).

Figure 2b shows a typical (V, I) characteristic taken at t = 25 ms for a probe located in this case 10 cm inside the outer limiter (i.e. 25 cm from the chamber outer wall). The electron and ion saturation current regimes can be seen at V > 100 V; also observable is a characteristic space potential of $\phi_s = +70 \pm 20$ V and a $T_e \cong 50$ eV (the Thompson-scattering T_e was only measured at the plasma centre and amounted to ≅100 eV). The absolute density inferred from the electron saturation currents using *un*magnetized probe theory is typically a factor of three lower than that obtained by the 2-mm microwave interferometer measurements. (Note that the probe signals appearing before the current rise are due to electrical pick-up of the breakdown oscillator and not to the plasma, and that the oscillator is terminated a few milliseconds after breakdown).

The behaviour of $\tilde{n}$ and $\tilde{\phi}_c$ with increasing density can also be seen in Fig.2a. Assuming from now on that the fluctuating component of the electron saturation current indicates $\tilde{n}$ (and not $\tilde{T}$), we roughly find $\tilde{n} \propto n^{\frac{1}{2}}$ ($\sqrt{T} \approx$ const during the density rise). The increase in n causes a decrease in $\tilde{\phi}_c$ such as expected from $\tilde{\phi}/T \propto \tilde{n}/n$ for this scaling. Measurement of the floating-potential fluctuations $\tilde{\phi}_f$ quantitatively confirms this, i.e. $\tilde{\phi}_{f,rms} \cong 10$ V when $T_e \cong 50$ eV and

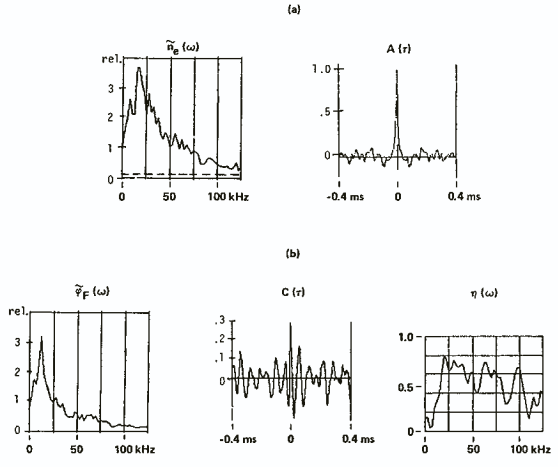

FIG.3. Analysis of electrostatic fluctuations: a) Typical spectrum of $\tilde{n}_e$ and its auto-correlation function A(τ), in this case for a probe 10 cm inside the outer limiter at t ≅ 30 ms into a discharge like that in Fig.2. Drum noise level is shown by the dashed line. b) Cross-correlation analysis between the probe used to measure $\tilde{n}_e$ in a) and another nearby probe measuring $\tilde{\phi}_f$.

$\tilde{n}_{rms}/n \cong 0.2$. Note that although the density in this particular discharge is increasing at the probe from $t \cong 10$ to $t \cong 30$ ms, the probe data at any given density have been checked to be the same as those of a 'steady-state' plasma maintained at that density. Note also that after $t = 30$ ms the electron saturation current begins to fall (even though the line-averaged density through the centre is still increasing), because of an inward movement of the plasma which starts at this time.

Further analysis of electrostatic fluctuations has been made along the same lines as described previously [1] (see also, e.g. Ref.[24]). Fourier spectra, auto- and cross-correlation functions, total and frequency-resolved correlation coefficients are computed in all cases below, using an averaging interval of $T = 4$ ms for each analysis, with slide-averaging in frequency over $\Delta f = 2$ kHz for the spectra and frequency-resolved correlation coefficient.

A typical spectrum of $\tilde{n}_e$ from the electron saturation current fluctuations of a Langmuir probe is shown in Fig.3a, along with its auto-correlation function $A(\tau) = (1/T) \int \tilde{n}(t)\, \tilde{n}(t-\tau)dt$. We have generally found that the spectral shapes of $\tilde{n}_e$, $\tilde{n}_i$, $\tilde{\phi}_c$ and $\tilde{\phi}_f$ are all similar and, further, that this spectral shape is roughly independent of n and of the radial position in the plasma (see Section 4.6). No time-independent or shot-to-shot reproducible mode structure above $f \cong 10$ kHz has been found, and the short auto-correlation time $\tau_A \cong 20\ \mu$s suggests a turbulent nature for these fluctuations.

Another result concerning the electrostatic fluctuations is shown in Fig.3b. At the left is the spectrum of floating-potential fluctuations $\tilde{\phi}_f$ as measured by a second Langmuir probe <0.5 cm away from the $\tilde{n}_e$ probe used in Fig.3a. Although the spectra of $\tilde{\phi}_f$ and $\tilde{n}$ are quite similar, we have found that there is only a partial correlation between the $\tilde{n}$ and $\tilde{\phi}_f$ as measured by two such nearby probes. The cross-correlation coefficient $C(\tau)$ and the frequency-resolved correlation coefficient $\eta(\omega)$ between $\tilde{n}$ and $\tilde{\phi}_f$ are defined as:

$$C(\tau) = \frac{1}{T}\int_0^T \tilde{n}(t)\,\tilde{\phi}_f(t-\tau)dt$$

$$\eta(\omega) = |\langle \tilde{n}(\omega)^* \tilde{\phi}_f(\omega)\rangle| / \sqrt{\langle \tilde{n}^2(\omega)\rangle \langle \tilde{\phi}_f^2(\omega)\rangle}$$

In the typical case shown in Fig.3b, the total frequency-averaged cross-correlation coefficient (which is the normalized peak value of $C(\tau)$) is only 29%. This indicates a substantial de-correlation between $\tilde{n}$ and $\tilde{\phi}_f$ (a total correlation coefficient of ~20% would indicate nearly complete de-correlation, while ≳60% indicates substantial correlation). Also, the frequency-resolved analysis at the right of Fig.3b indicates that this lack of complete correlation between $\tilde{n}$ and $\tilde{\phi}_f$ is characteristic of fluctuations over the whole band $f < 100$ kHz (note that $\eta(\omega)$ is a narrow-band coefficient evaluated over an interval of $\Delta\omega = 2$ kHz and for $\tau = 0$).

Thus the prediction of simple electrostatic models that $\tilde{\phi}$ and $\tilde{n}$ are intrinsically correlated does not appear to be valid for this plasma. This could be due to nonlinear effects ($\tilde{n}/n > 0.1$) or, possibly, to an independent temperature fluctuation with a spectrum similar to that of $\tilde{n}$.

4. COMPARISON OF ELECTROSTATIC AND MAGNETIC FLUCTUATIONS

4.1. Radial profiles

The radial profiles of $\tilde{B}_r$ and $\tilde{n}/n$ reported in Ref.[1] are reproduced in the present experiment, with the difference that the RF antenna has moved the effective outer limiter of the plasma from the outer wall to a point 15 cm inside the wall, as can be seen in Fig.4a.

The profile of $\tilde{n}/n$ as shown in Fig.4b is peaked near the outside, whereas the profiles of n and $\tilde{B}_r$ are similar and increasing towords the centre of the plasma. Note that we are assuming that $\tilde{T} = 0$ and that the profile of the electron saturation current is roughly equivalent to the profile of n, i.e. that the temperature profile is approximately the same as the density profile. Also shown in this figure is the profile of space potential from the (V, I) Langmuir probe characteristic. The space potential is nearly constant over the range of radii probed and is also nearly constant over the density range of Macrotor.

The amplitude of fluctuations at about 15 cm inside the outer limiter is typically $\tilde{B}_{r,rms}/\tilde{B}_T \cong 10^{-4}$ (excluding low-frequency components at $f \leqslant 20$ kHz) and $\tilde{n}_{rms}/n \cong 10\%$. In the diffuse-shadow region behind the RF antenna boundary, the density and $\tilde{B}$ fluctuation levels fall off monotonically as shown in Fig.4a, while the relative density fluctuation level remains high. The spectrum of $\tilde{B}_r$ observed in this edge region is similar to that observed further into the plasma, except for a relative decrease in the level of high-frequency components nearer the wall. The

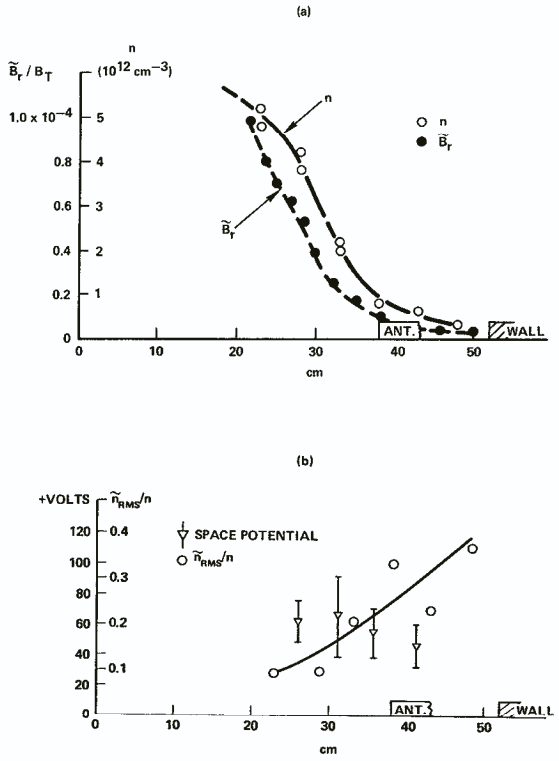

FIG.4. Radial profiles: a) Profiles of n (actually electron saturation current) measured with a Langmuir probe and $\tilde{B}_r$ (summed over all frequencies in a discharge without the low-frequency mode). b) Profiles of space potential ϕ_s and $\tilde{n}_{rms}/n$. All profiles are measured at a fixed time in discharges with $\bar{n}_e = 4 \times 10^{12}\ cm^{-3}$ through the minor axis. Ion saturation current profiles of $\tilde{n}/n$ are also similar to those shown here.

spectrum of $\tilde{n}$ behind the antenna is still broadband and monotonically decreasing with frequency, but the $\tilde{n}$ and $\tilde{\phi}$ have a non-Gaussian ('spikey') amplitude distribution nearer to the wall.

This similarity in the fluctuation spectra observed over a factor ~10 in density (from the edge to near the middle of the plasma) is also observed when the density at a fixed probe is varied during a single discharge (see Section 4.6). Both these results indicate that these spectra are apparently insensitive to density, i.e. to collisionality in the Macrotor plasma. In addition, the existence of fluctuations in the geometrical shadow of the limiter indicates that an ideal flux surface is not necessary to support these fluctuations.

4.2. Cross-correlation

The relationship between $\tilde{\phi}_c$ and $\tilde{B}_r$ can be studied most directly by measuring the cross-correlation between these two signals. In Fig.5a, we show an example of the general result that no significant correlation is detectable between $\tilde{\phi}_c$ and $\tilde{B}_r$ as measured by two probes at the same 'point' (as in Fig.1). The correlation coefficient $\eta(\omega) \cong 0.2$ is nearly as low as that characteristic of two independent noise sources, and the cross-correlation function $C(\tau)$ has no structure which would indicate a significant linear relationship between the two signals.

A similar lack of correlation has been found between $\tilde{B}_r$ and $\tilde{\phi}_c$, and $\tilde{B}_p$ and $\tilde{\phi}_c$ or $\tilde{\phi}_c$ when the capacitive and magnetic probes are either together or separated from each other radially or poloidally. In addition, floating-potential fluctuations $\tilde{\phi}_f$ measured by a Langmuir probe just outside the $\dot{B}$ coil showed no correlation between $\tilde{\phi}_f$ (or $\tilde{\phi}_f$) and $\tilde{B}_p$ (or $\tilde{B}_r$).

4.3. Spectra

Figure 5b shows a comparison of the spectral shape of $\tilde{\phi}_c$ and $\tilde{B}_r$ obtained from probes such as used to

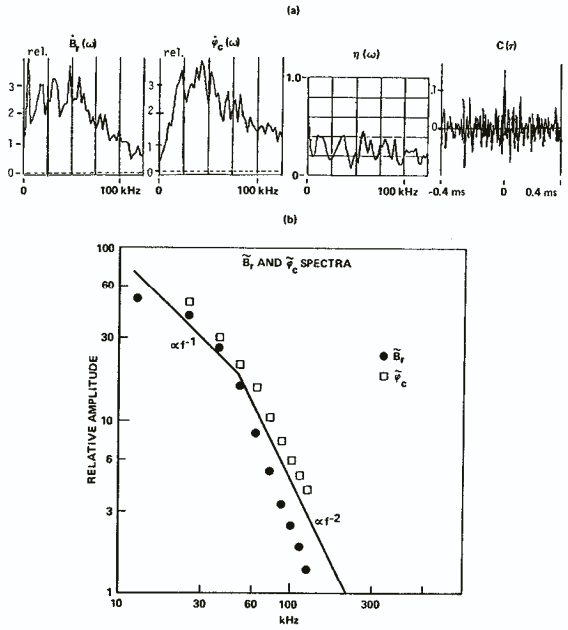

FIG.5. a) Cross-correlation between $\tilde{B}_r$ and $\tilde{\phi}_c$: typical spectra of $\tilde{B}_r$ and $\tilde{\phi}_c$ are shown along with $C(\tau)$ and $\eta(\omega)$ for a magnetic and capacitive probe at the same 'point'. The total cross-correlation coefficient between the two signals is 0.17, which is nearly as low as that of two independent noise sources. b) log-log plot of spectral shapes of $\tilde{B}_r$ and $\tilde{\phi}_c$. For these cases, $\bar{n} = 4 \times 10^{12}\ cm^{-3}$ through the centre of the plasma, but similar results hold throughout the density range of Macrotor.

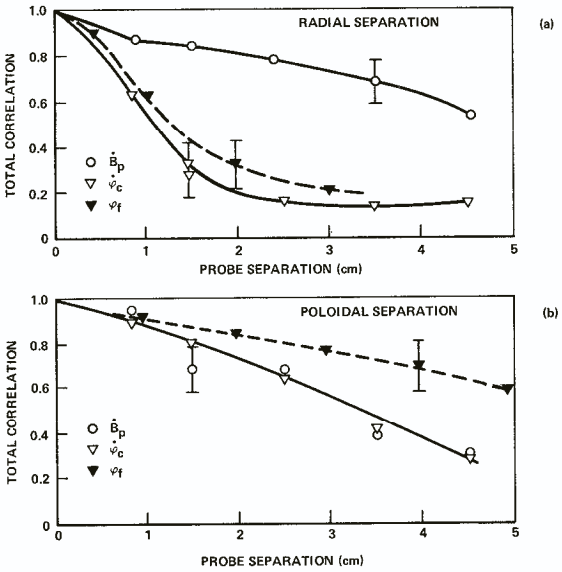

FIG.6. Correlation lengths: total correlations C(0) versus radial (a) and poloidal (b) probe separations. For $\tilde{B}$ we have $L_r \approx L_p \ll L_T$, while for $\tilde{\phi}$, we have $L_r < L_p \ll L_T$. The radial and poloidal correlations of $\tilde{B}_r$ and $\tilde{B}_p$ are similar to one another; the toroidal correlation lengths of $\tilde{B}$ and $\tilde{\phi}$ are both $\gg 5$ cm.

evaluate the cross-correlation shown in Fig.5a. The two spectra consistently show an overall similarity in that they are both broadband and monotonically decreasing with frequency, but at high frequencies, f>50 kHz, $\tilde{B}_r$ falls with frequency a bit faster than $\tilde{\phi}_c$. Note that a large low-frequency mode (Mirnov oscillation) at f ≅ 10 kHz can appear in $\tilde{B}_r$ and sometimes in $\tilde{\phi}$, but this mode has apparently no connection with the ubiquitous broadband higher-frequency structure.

4.4. Correlation lengths

A simple measure of correlation lengths can be obtained by varying the separation x between two probes of the same type located inside the same glass tube. In Fig.6a, we show the total correlation versus x for $\tilde{B}_r$ and $\tilde{\phi}_c$ for radial separations as measured by probes in a horizontal tube at a point ≅10 cm inside the outer limiter, and in Fig.6b, we show the total correlation versus x for $\tilde{B}_r$ and $\tilde{\phi}_c$ for poloidal probe separations measured near the equatorial plane in a vertical tube located approximately at the outer limiter boundary. The error bars indicate typical shot-to-shot variability.

It can be seen that the radial correlation between the two ϕ_c probes falls with separation faster than the radial correlation between the two B_r probes, indicating that the averaged radial correlation length L_r for ϕ_c is smaller than that of B_r. On the other hand, the poloidal correlation lengths of B_p and ϕ_c are similar to each other and to the radial correlation length of B_r. This difference between L_r and L_p for the electrostatic fluctuations is confirmed by Langmuir probe measurements of floating-potential $\tilde{\phi}_f$, as is also shown in Fig.6. The frequency dependencies of the poloidal correlation lengths of $\tilde{\phi}_c$ and $\tilde{B}_r$ are both similar to that reported previously for $\tilde{B}_r$ [1], i.e. the correlation lengths are monotonically decreasing with frequency and are 5–7 cm at 50 kHz and $n_e(0) \sim 5 \times 10^{12}$ cm^{-3}.

4.5. Phase velocity

The poloidal phase velocity can be measured by examining the relative phase ΔΦ versus frequency between two probes as their poloidal separation x is varied, the velocity being given by $v_p = 2\pi xf/\Delta\Phi$. As the probes are separated, their cross-correlation begins to deteriorate, particularly at higher frequencies, so that a consistent phase difference can only be identified over a limited range of x and f. We have, however, roughly found $v_p \cong 0.5$–1×10^6 cm·s^{-1} in the electron diamagnetic direction for electrostatic fluctuations as measured by both the capacitive and Langmuir probes, compared with $v_p \cong 1$–2×10^6 cm·s^{-1} in the same direction for $\tilde{B}_p$ fluctuations. Thus, there seems to be a possible difference between the rotation velocities for the two types of disturbances although the uncertainties involved do not allow a precise statement of this comparison.

4.6. Variation with density

We have found that $\tilde{n}$ increases with n when the plasma density at a fixed probe is increased (Fig.2), while the spectrum of $\tilde{n}$ remains roughly invariant (although there is a tendency for the peak to shift upward in frequency to ~40 kHz at the highest densities). For $\tilde{B}$ fluctuations, both the spectrum and amplitude remain nearly constant as n is increased. The most noticeable change in $\tilde{B}$ with density is a decrease in the radial correlation length of $\tilde{B}_r$. Note that these results for fluctuations in the region 10–15 cm inside the outer limiter boundary are not sufficient to attempt to define a global scaling law which might be related to the gross energy confinement scaling.

5. DISCUSSION

In spite of a small residual uncertainty concerning probe perturbation effects, the information of Section 4 can be regarded as a rather conclusive indication of the absence of a clear-cut relationship between the broadband magnetic and electrostatic fluctuations in this frequency range in a tokamak. On the other hand, the similarity of $\tilde{B}$ and $\tilde{\phi}$ spectra and of their poloidal correlation lengths seems to suggest that there may be a more subtle connection between the two than is presently evident.

A somewhat independent check of these results has come from probe measurements on other tokamaks. For example, experiments on the Caltech tokamak [5, 9, 22] have had results which agree at several points with those described here, e.g. on the magnitudes of $\tilde{n}/n$ and $\tilde{B}_r/B_T$, on the broadband nature and similarity of the spectra of $\tilde{B}$ and $\tilde{n}$, on the positive space potential, and on the correlation length ordering $L_r < L_p$. There are, however, also some points of difference [5], e.g. some low-frequency mode structure has been observed in the electrostatic spectrum, and a difference in the spectra of $\tilde{B}_p$ and $\tilde{B}_r$ has been noted [22]. Also relevant as a check of these results is a probe experiment on the TOSCA tokamak [8] indicating the presence of small-scale broadband magnetic fluctuations inside the plasma. Note that in none of these experiments does there appear to be a connection between the low-frequency Mirnov oscillation and the broadband higher-frequency fluctuations.

There seem to be, at least, two possible interpretations of the basic result, i.e. the partial dissimilarity between magnetic and electrostatic fluctuations: (1) that the magnetic and electrostatic components of a single instability are non-linearly or non-locally related; (2) that there are separate magnetic and electrostatic instabilities, e.g. driven by temperature [17] and density gradients. We also note the possibility that part of the de-correlation may be due to a difference between the correlation lengths of $\tilde{B}$ and $\tilde{\phi}$ components of a single type of instability (such that, e.g. the probes respond to a different effective volume for $\tilde{B}$ and $\tilde{\phi}$ fluctuations). Although the short correlation lengths and times and the absence of any persistent mode structure might seem to favour a stochastic field model [11, 12], there is as yet no direct experimental test of stochasticity (e.g. by following a field toroidally around the machine).

Finally, it should be noted that no direct experimental connection between these fluctuations and transport has been made. Such a connection is difficult to establish without active control of the fluctuations; for example, a fluctuation scaling such as $\tilde{n}/n \propto n^{-\frac{1}{2}}$ might suggest that the transport associated with $\tilde{n}$ decreases with density like empirical scaling, but it could also be true that the change in $\tilde{n}$ is an artifact of some other change in the plasma caused by varying n, such that the variation of $\tilde{n}$ has no causal relation to the empirical scaling.

ACKNOWLEDGEMENTS

We thank C.R. Menyuk for his contributions to the formulation of the data analysis and D. Whelan for assistance in data taking. Also we thank the theorists (particularly, J.F. Drake) with whom we have discussed these results.

REFERENCES

[1] ZWEBEN, S.J., MENYUK, C.R., TAYLOR, R.J., Phys. Rev. Lett. **42** (1979) 1270.
[2] SLUSHER, R.E., SURKO, C.M., Phys. Fluids **23** (1980) 472, and references therein.
[3] MAZZUCATO, E., Phys. Fluids **21** (1978) 1063.
[4] SEMET, A., MASE, A., PEEBLES, W.A., LUHMANN, N.C., ZWEBEN, S.J., Phys. Rev. Lett. **45** (1980) 445.
[5] KUBENA, R.L., Ph.D. Thesis, California Institute of Technology, Pasadena (1978).
[6] OHTSUKA, H., KIMURA, K., SHIMOMURA, S., MAEDA, H., YAMAMOTO, S., NAGAMI, M., UEDA, N., KITSUNEZAKI, A., NAGASHIMA, T., Plasma Phys. **20** (1978) 749.
[7] HORTON, W., ESTES, R.D., Nucl. Fusion **19** (1979) 203; CHENG, C.Z., OKUDA, H., Nucl. Fusion **18** (1978) 587.
[8] ROBINSON, D.C., McGUIRE, K., Nucl. Fusion **19** (1979) 115.
[9] HEDEMANN, M., PhD Thesis, California Institute of Technology (1981). (See also Ref.[22]).
[10] CALLEN, J.D., Phys. Rev. Lett. **39** (1977) 1540.
[11] STIX, T.H., Nucl. Fusion **18** (1978) 353.
[12] RECHESTER, A.B., ROSENBLUTH, M.N., Phys. Rev. Lett. **40** (1978) 38.
[13] MOLVIG, K., RICE, J.E., TEKUDA, M.S., Phys. Rev. Lett. **41** (1978) 1240.
[14] LIN, A.T., DAWSON, J.M., OKUDA, H., Phys. Rev. Lett. **41** (1978) 753.
[15] MOLVIG, K., HIRSHMAN, S.P., WHITSON, J.C., Phys. Rev. Lett. **43** (1979) 583.
[16] MANNHEIMER, W., COOK, I., Comments Plasma Phys. Controlled Fusion **5** (1979) 9.
[17] DRAKE, J.F., GLADD, N.T., LIU, C.S., CHANG, C.L., Phys. Rev. Lett. **44** (1980) 994.
[18] CHU, M.S., CHU, C., HSU, J.Y., General Atomic Report GA-A15273 (1979).

[19] MYNICK, H.E., KROMMES, J.A., Princeton Plasma Physics Lab. Report PPPL-1556 (1979).
[20] KADOMTSEV, B.B., POGUTSE, O.P., in Plasma Physics and Controlled Nuclear Fusion Research (Proc. 7th Int. Conf. Innsbruck,1978) Vol.1, IAEA, Vienna (1979) 649.
[21] MOLVIG, K., CHANG, C.L., DRAKE, J.F., GLADD, N.T., GUZDAR, P., HASSAM, A., HIRSHMAN, S.P., LEE, Y.C., LIU, C.S., MARCHAND, R., RECHESTER, A.B., ROSENBLUTH, M.N., WHITE, R.B., in Plasma Physics and Controlled Nuclear Fusion Research (Proc. 8th. Int. Conf. Brussels, 1980) to appear.
[22] TAYLOR, R.J., GOULD, R.W., HEDEMANN, M.A., LEE, P., LEVINE, B.S., LUHMANN, N.C., Jr., MASE, A., MORALES, G.J., PEEBLES, W.A., SEMET, A., SCHWIRZKE, F., TALMADGE, S., ZWEBEN, S.J., ibid.
[23] ROTH, J.R., KRAWCZONEK, W., Rev. Sci. Instrum. **42** (1971) 589.
[24] BENDAT, J.S., PIERSOL, A.G., Random Data, Interscience, New York (1971).

(Manuscript received 3 March 1980
Final manuscript received 25 November 1980)